Spin-lattice relaxation in the mixed state of the high-T_c cuprates: Electronic spin-flip scattering versus spin fluctuations

Dirk K. Morr
Theoretical Division, MS B262, Los Alamos National Laboratory, Los Alamos, New Mexico 87545
(Received 19 July 2000; published 8 May 2001)

Recent experimental and theoretical studies have established that the spin-lattice relaxation rate $1/T_1$ measured in nuclear magnetic resonance (NMR) experiments is a site-sensitive probe for the electronic spectrum in the mixed state of the high-T_c cuprates. While some groups suggested that $1/T_1$ is solely determined by spin-flip scattering of BCS-like electrons, other groups stressed the importance of antiferromagnetic spin-fluctuations. We show that these two relaxation mechanisms give rise to a *qualitatively* different temperature and frequency dependence of ^{17}O $1/T_1$. A comparison of our results with the experimental ^{17}O $1/T_1$ data provides support for a relaxation mechanism dominated by antiferromagnetic spin fluctuations.

DOI: 10.1103/PhysRevB.63.214509 PACS number(s): 74.25.Nf, 74.60.Ec, 74.25.Ha

Recently the temperature and frequency dependence of the ^{63}Cu and ^{17}O spin-lattice relaxation rate $1/T_1$ in the mixed state of $YBa_2Cu_3O_{6+x}$ (YBCO) has been the focus of intense experimental efforts.[1–4] It was first shown by Curro *et al.* (CMHS),[1,2] and subsequently by Halperin *et al.*[4] that ^{17}O $1/T_1$ in the mixed state of $YBa_2Cu_3O_7$ increases with increasing resonance frequency, i.e., with decreasing distance from the vortex core. Preliminary results of Milling *et al.*[3] show a qualitatively similar behavior for the ^{63}Cu relaxation rate in YBCO. CMHS were the first to point out that this frequency dependence of $1/T_1$ arises from the presence of a supercurrent, which gives rise to a site-specific density of states, and consequently a site-specific $1/T_1$. This interpretation receives strong support from the experimental observation that the frequency dependence of $1/T_1$ disappears above the melting temperature of the vortex lattice.

Several theoretical models[5–7] have been suggested to explain the experimentally observed frequency dependence of $1/T_1$. Using a weak coupling approach, it was argued in Refs. 5,7 that $1/T_1$ for ^{63}Cu arises solely from electronic spin flip (ESF) scattering of BCS-type electrons. In contrast, Morr and Wortis (MW)[6] proposed a strong coupling scenario in which antiferromagnetic spin fluctuations (ASF) and their interaction with the electronic degrees of freedom provide the dominant contribution to the ^{63}Cu spin-lattice relaxation rate. MW also conjectured that the combined temperature and frequency dependence of $1/T_1$ can distinguish between relaxation due to electronic spin-flip scattering and relaxation due to antiferromagnetic spin fluctuations.

In this paper we present detailed predictions for the temperature and frequency dependence of the ^{17}O spin-lattice relaxation rate in the frameworks of the weak coupling ESF and strong coupling ASF approach. We show that due to the specific form of the ^{17}O hyperfine coupling, the temperature and frequency dependence of the ^{17}O $1/T_1$ for ESF and ASF relaxation is *qualitatively* different. In particular, we demonstrate that for the ESF mechanism, $1/T_1$ increases monotonically with temperature and possesses a large distribution of values, for a given resonance frequency, close to the vortex core. In contrast, for the ASF relaxation mechanism, we obtain a well-defined relation between $1/T_1$ and resonance frequency, and a nonmonotonic dependence of $1/T_1$ on temperature. Though a comparison of our theoretical results with the available experimental data suggests that the spin-lattice relaxation rate in the mixed state is dominated by the ASF mechanism, further experiments are required to test the predictions presented in this paper. To the extent that future experiments confirm our conclusion, it immediately implies that the relaxation rate of ^{63}Cu is as well dominated by antiferromagnetic spin fluctuations due to its even more favorable hyperfine coupling.

We begin by shortly reviewing the theoretical models for an ESF and ASF based spin-lattice relaxation rate; a detailed account is given in Refs. 5–7. For ESF relaxation,[8] we consider the model of Ref. 7, whose results are in good qualitative with those presented in Ref. 5.

The general expression for the ^{17}O spin-lattice relaxation rate $1/T_1$ with an applied field parallel to the c axis is given by

$$\frac{1}{T_1T}=\frac{k_B}{2\hbar}(\hbar^2\gamma_n\gamma_e)^2\frac{1}{N}\sum_{\mathbf{q}}F_{\mathrm{O}}(\mathbf{q})\lim_{\omega\to 0}\frac{\chi''(\mathbf{q},\omega)}{\omega}, \quad (1)$$

where

$$F_{\mathrm{O}(2)}(q)=C^2\cos(q_x/2)^2 \quad F_{\mathrm{O}(3)}(q)=C^2\cos(q_y/2)^2, \quad (2)$$

C is the ^{17}O transferred hyperfine coupling constant, and O(2)[O(3)] is the planar oxygen nucleus which is located between two Cu nuclei along the $x(y)$ axis.

Within the ESF approach the spin-susceptibility in the superconducting state, neglecting final state effects, is given by $\chi=\Sigma$, where

$$\Sigma(\mathbf{q},i\omega_n)=-T\sum_{\mathbf{k},m}\{G(\mathbf{k},i\Omega_m)G(\mathbf{k}+\mathbf{q},i\Omega_m+i\omega_n) + F(\mathbf{k},i\Omega_m)F(\mathbf{k}+\mathbf{q},i\Omega_m+i\omega_n)\}, \quad (3)$$

and G and F are the normal and anomalous Green's functions

$$G(\mathbf{k},i\Omega_m)=\frac{v_{\mathbf{k}}^2}{i\Omega_m-E_{\mathbf{k}}}+\frac{u_{\mathbf{k}}^2}{i\Omega_m+E_{-\mathbf{k}}},$$

$$F(\mathbf{k},i\Omega_m)=-u_{\mathbf{k}}v_{\mathbf{k}}\left\{\frac{1}{i\Omega_m-E_{\mathbf{k}}}-\frac{1}{i\Omega_m+E_{-\mathbf{k}}}\right\}. \quad (4)$$

In the limit that the supercurrent momentum $\mathbf{p}_s$ varies on a length scale larger than $1/k_F$, the dispersion of the fermionic quasiparticles $E_{\mathbf{k}}$ up to linear order in p_s is in semiclassical approximation given by[9]

$$E_{\mathbf{k}}=\sqrt{\epsilon_{\mathbf{k}}^2+|\Delta_{\mathbf{k}}|^2}+\mathbf{v}_F(\mathbf{k})\cdot\mathbf{p}_s, \quad (5)$$

where $\epsilon_{\mathbf{k}}$ is the electronic normal state dispersion, $\Delta_{\mathbf{k}}=\Delta_0[\cos(k_x)-\cos(k_y)]/2$ is the *d*-wave gap, and $\mathbf{v}_F(\mathbf{k})=\partial\epsilon_{\mathbf{k}}/\partial\mathbf{k}$. Following MW, we neglect the electronic Zeeman splitting which for typical applied fields is much smaller than the second term in Eq. (5), the so-called Doppler shift, as well as any effects of the supercurrent on $\Delta_{\mathbf{k}}$, $u_{\mathbf{k}}$, and $v_{\mathbf{k}}$.[10]

Spin relaxation due to the ASF mechanism is described by the spin-fermion model[11] where the spin susceptibility χ is renormalized by the interaction with low-energy fermionic degrees of freedom and given by

$$\chi^{-1}=\chi_0^{-1}-\Pi. \quad (6)$$

Here

$$\chi_0^{-1}=\frac{\xi_0^{-2}+(\mathbf{q}-\mathbf{Q}_i)^2}{\alpha}, \quad (7)$$

is the bare propagator, ξ_0 is the *bare* magnetic correlation length in units of the lattice constant a_0, α is a temperature independent constant, $\mathbf{Q}=(\pi,\pi)$ is the position of the magnetic peak in momentum space,[12] and Π is the bosonic self-energy given by the irreducible particle-hole bubble. A supercurrent affects χ only through Π, which is calculated using second order perturbation theory in the spin-fermion coupling *g*, and one obtains

$$\Pi=g^2\Sigma, \quad (8)$$

with Σ in Eq. (3). In the limit $\omega\to 0$, $\mathrm{Re}\,\Pi$ is only weakly momentum dependent and can thus be included in a renormalized but momentum independent correlation length ξ in Eq. (7).

For both the ESF and ASF mechanisms, we are thus left with the calculation of $\mathrm{Im}\,\Sigma$ which for $\omega\to 0$ is dominated by particle-hole excitations in the vicinity of the superconducting nodes. Expanding $E_{\mathbf{k}}$ up to linear order in momentum around the nodes, we can perform the momentum and frequency integrations in Eq. (3) analytically. Combining the resulting expression for $\mathrm{Im}\,\Sigma$ with Eqs. (1), (6), and (7) we obtain the spin-lattice relaxation rate presented in Eq. (A1) of the Appendix. For our subsequent discussion of the ESF and ASF mechanism it is necessary to briefly review the form of $1/T_1$ in two limits. A low temperatures where $|D_m/T|\gg 1$ for $m=1\cdots 4$, one obtains from Eq. (A1)

$$\frac{1}{T_1T}=A\left(\frac{1}{v_Fv_\Delta}\right)^2\sum_{n,m}\left\{\mathcal{F}(\mathbf{q}_{n,m})\left(D_mD_n+\frac{\pi^2T^2}{3}\right)+\mathcal{F}(\mathbf{q}_{n,m+2})\left(D_mD_n-\frac{\pi^2T^2}{3}\right)\right\}+O(e^{D_m/T}), \quad (9)$$

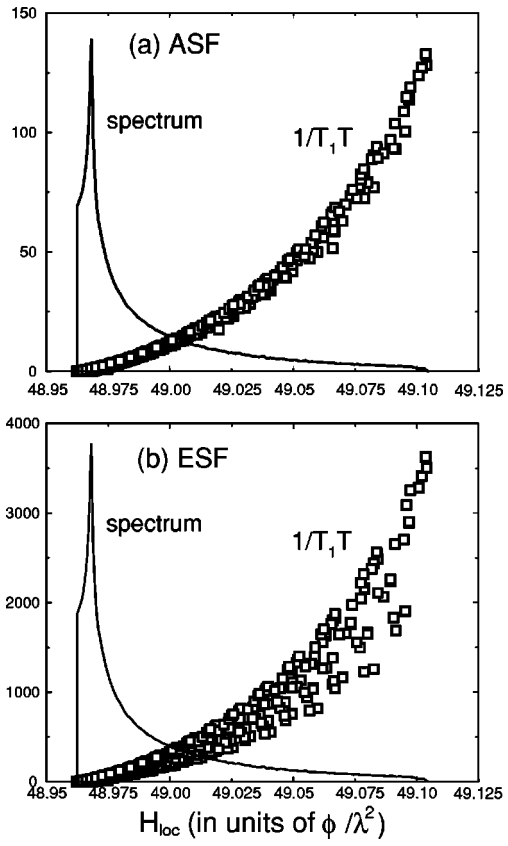

FIG. 1. ^{17}O spectrum (solid line) together with ^{17}O(2,3) $(1/T_1T)$ as a function of local magnetic field H_{loc}, for $T=1$ K. (a) ASF mechanism and (b) ESF mechanism.

where $\mathcal{F}(\mathbf{q}_{n,m}),D_m,A$, and v_Δ are defined in the Appendix, and the sum runs only over those nodes with $D_m,D_n<0$. Since the supercurrent in general breaks the lattice symmetry, the O(2) and O(3) relaxation rates are expected to be different, as we shall discuss below. In contrast, in the high-temperature limit ($|D_m/T|\ll 1$ for $m=1\cdots 4$) one has

$$\frac{1}{T_1T}=A\frac{\pi}{3}\left(\frac{T}{v_Fv_\Delta}\right)^2\sum_{n,m=1}^{4}\mathcal{F}(\mathbf{q}_{n,m}) \quad (10)$$

and we recover the temperature dependence of the relaxation rate in the absence of a supercurrent.

A site specific relation between the resonance frequency $\Delta\nu(\mathbf{r})=\gamma_n\hbar H_{\mathrm{loc}}(\mathbf{r})$, where γ_n is the ^{17}O nuclear gyromagnetic ratio and $H_{\mathrm{loc}}(\mathbf{r})$ is the local magnetic field, and $1/T_1$ is obtained via the local supercurrent momentum $\mathbf{p}_s(\mathbf{r})\sim\nabla\times\mathbf{H}_{\mathrm{loc}}(\mathbf{r})$; a relation which is valid even in the presence of nonlocal as well as nonlinear corrections.[13] Following MW, we restrict our discussion of the relaxation rates to nuclei which are further than $R>2\xi_{ab}$ from the center of the vortex core (where ξ_{ab} is the superconducting in-plane coherence length).[14] We consider a hexagonal vortex lattice[15,16] and use the parameter set $v_F\approx 0.4$ eV, $v_\Delta\approx 20$ meV, and $\xi\approx 2$,[17] which was shown to describe fermionic and magnetic excitations in $YBa_2Cu_3O_7$.[6,12]

In Fig. 1 we plot the ^{17}O spectrum[6] which describes the

distribution of local magnetic fields (solid line) and ^{17}O(2,3) $1/T_1T$ (open squares) for (a) the ASF mechanism and (b) the ESF mechanism as a function of $H_{\rm loc}$, i.e., resonance frequency. Nuclei at the highest frequencies are located at a distance $2\xi_{ab}$ from the center of the vortex (nuclei closer to the vortex core have been omitted, see above discussion), nuclei at the lowest frequencies are in the center of a vortex triangle, those at the maximum of the spectrum are at the midpoint between two vortices.

For both relaxation mechanisms, $1/T_1T$ increases with increasing resonance frequency, i.e., decreasing distance from the vortex core, similar to the results obtained in Refs. 5–7 for ^{63}Cu. For $T=1$ K, the relaxation rate for practically all nuclei is given by $1/T_1T \sim p_s^2$, Eq. (9), and since $|\mathbf{p}_s|$ increases with decreasing distance from the vortex core $1/T_1T$ increases consequently. However, $1/T_1T$ for the ESF mechanism exhibits a large distribution of values for a given $H_{\rm loc}$, in contrast to $1/T_1T$ for ASF relaxation. Nuclei with the same resonance frequency can in general possess different relaxation rates, since $1/T_1T$ depends not only on the magnitude of $\mathbf{p}_s$, but also on the angle between the direction of the local supercurrent and the crystal axes, i.e., the Fermi velocity v_F at the nodal points, Eq. (9). It is exactly this angular dependence which for ESF relaxation leads to the large distribution of values for $1/T_1T$. The absence of such a large distribution for the ASF mechanism is due to the antiferromagnetic enhancement factor (i.e., the Stoner enhancement) in the denominator of Eq. (A3).

The Stoner enhancement favors particle-hole excitations which connect nodes at opposite sites of the Fermi surface (FS), i.e., with large momentum transfer, $q_{n,m}=\mathbf{k}_l$ [see Fig. 2(a)]. Due to this enhancement, the second term on the right-hand side (RHS) of Eq. (9) yields the dominant contribution to $1/T_1T$ for ASF relaxation in the low-temperature limit, and one obtains

$$\frac{1}{T_1T} \approx A\left(\frac{1}{v_F v_\Delta}\right)^2 \mathcal{F}(\mathbf{k}_l)(\mathbf{v}_F^2\mathbf{p}_s^2 - 2\pi^2T^2/3). \qquad (11)$$

Thus the leading temperature contribution to $1/T_1T$ is independent of the angle between $\mathbf{p}_s$ and the underlying lattice, and the narrow distribution of $1/T_1T$ seen at higher frequencies for ASF relaxation arises solely from subleading contributions including particle-hole excitations with small momentum transfer, e.g., with $q_{n,m}=\mathbf{k}_s$ [see Fig. 2(a)].

In Fig. 3 we present the relaxation rates of the two planar oxygen nuclei ^{17}O(2,3) for three different temperatures (while the 30 and 60 K curves are horizontally offset for clarity, the right end points of all curves correspond to the same local field at a distance $2\xi_{ab}$ from the vortex core).

The temperature dependence of $1/T_1T$ in the ASF approach [Fig. 3(a)] is similar to that of ^{63}Cu shown in Fig. 2 of Ref. 6. With increasing temperature, $1/T_1T$ at high resonance frequencies decreases, in agreement with Eq. (11), while at low frequencies $1/T_1T \sim T^2$, Eq. (10), and the relaxation rate increases. As a result, $1/T_1T$ possesses a nonmonotonic dependence on the local field, as shown by the minimum in the relaxation rate for intermediate frequencies, which was discussed in detail in Ref. 6. Note that the overall

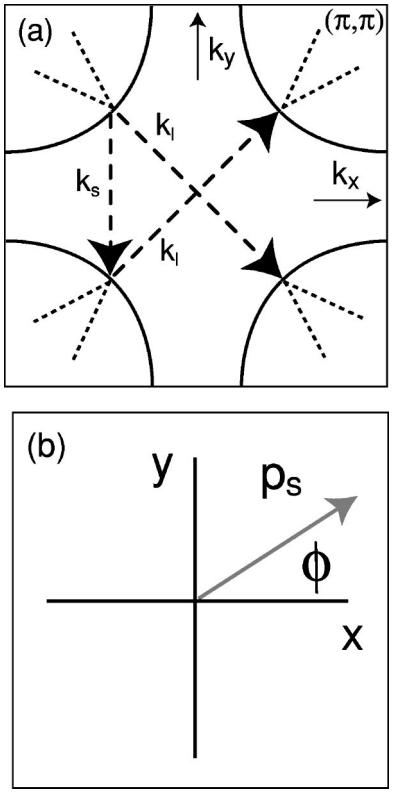

FIG. 2. (a) Fermi surface and particle-hole excitations (dashed arrow) with $q_{n,m}=\mathbf{k}_{l,s}$ (nodes of the superconducting gap are shown as dotted lines). (b) Angle between $\mathbf{p}_s$ and the crystal x axis.

prefactors $A_{\rm ASF}$ and $A_{\rm ESF}$, for ASF and ESF relaxation are different [see Eqs. (A2) and (A3) in the Appendix] and only insufficiently known such that a direct comparison of $1/T_1T$ in Figs. 3(a),3(b) in absolute units is not possible.

In contrast, $1/T_1T$ for the ESF mechanism increases with increasing temperature at all resonance frequencies. At low frequencies, i.e., in the high-temperature limit, this follows directly from Eq. (10). At higher frequencies, i.e., in the low-temperature limit, an analysis of Eq. (9) shows that due to the ^{17}O form factors, the first term on the RHS of Eq. (9) dominates $1/T_1T$ which therefore also increases with increasing temperature. Consequently, $1/T_1T$ does *not* exhibit a minimum as a function of the local field as was the case for ASF relaxation. Note also that the distribution of values for $1/T_1T$ decreases as the temperature increases, since in the high-temperature limit the relaxation rate becomes independent of resonance frequency, i.e., $1/T_1T \sim T^2$. The spin relaxation rate thus possesses *qualitatively* different frequency and temperature dependencies for the ASF and ESF mechanism, the origin of which lies in the antiferromagnetic enhancement factor in the denominator of Eq. (A3) which is only present for ASF relaxation. We next compare our theoretical results with the experimental data on ^{17}O(2,3) $1/T_1T$ by CMHS,[2] which we present in Fig. 4.

The experimentally measured $1/T_1T$ increases with increasing resonance frequency, in agreement with our theoretical results in Fig. 3, decreases between $T=5$ K and $T=10$ K with a larger reduction at higher frequencies, and

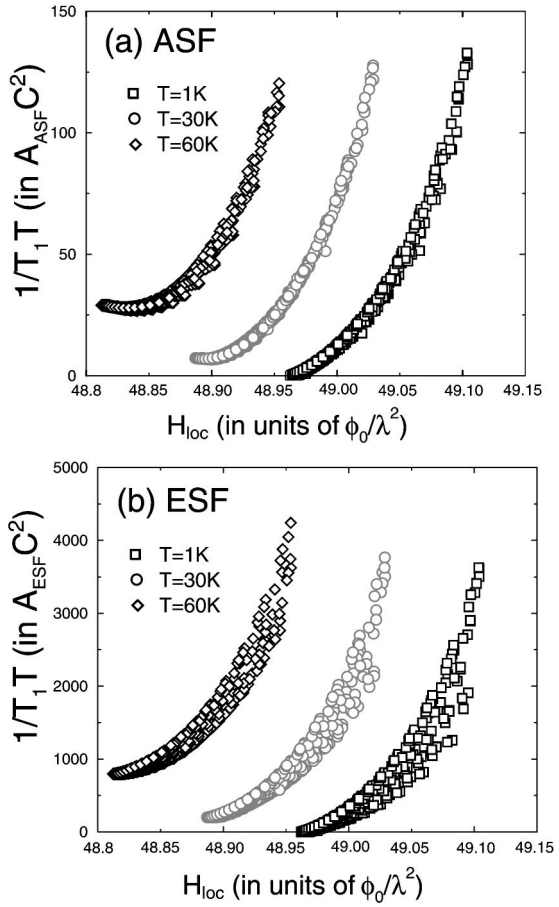

FIG. 3. ^{17}O(2,3) $(1/T_1T)$ as a function of local field for three different temperatures. (a) ASF mechanism, (b) ESF mechanism. The 30 and 60 K curves are horizontally offset for clarity.

increases between $T=10$ K and $T=40$ K. No evidence for a distribution of relaxation rates at high frequencies was found so far, however, a further quantitative analysis is still required to determine an upper bound for the spread in $1/T_1$.[18] Though both experimental features agree qualitatively with our theoretical predictions for $1/T_1T$ in the ASF approach [see Fig. 3(a)], spin-diffusion, impurity effects, and vortex vibrations[19] can potentially contribute to the spin-lattice relaxation and thus complicate the analysis of the experimental data within the ASF or ESF approach. While it was argued[7] that spin diffusion is strongly suppressed by the inhomogeneity of the magnetic field in a vortex lattice, CMHS concluded from the different temperature dependence of the apical and planar oxygen relaxation rates, that for $T \geqslant 25$ K vortex vibrations are irrelevant for the relaxation of ^{17}O; thus the relaxation arises solely from the electronic or magnetic mechanisms discussed above. For $T \leqslant 25$ K, the apical and planar oxygen relaxation rates exhibit the same linear temperature dependence, however, the planar $1/T_1$ is still considerably larger than the apical $1/T_1$. Though this result does not exclude the possibility that vortex vibrations contribute to the relaxation process below 25 K, it suggests that the relaxation mechanism is still dominated by electronic/magnetic excitations. Clearly, further measurements of $1/T_1T$ are required to study the various relaxation mechanisms.[20] However, to the extent that the effects of vortex vibrations and impurities are negligible at low temperatures, the experimental data in Fig. 4 support a predominant ASF mechanism of the spin relaxation in the mixed state.

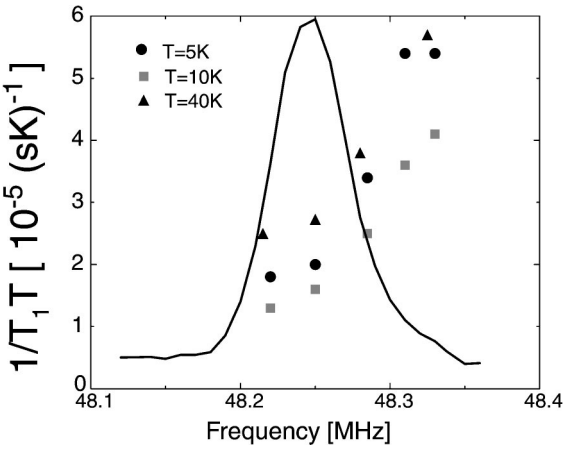

FIG. 4. Experimental data for the ^{17}O spectrum (solid line) together with $(1/T_1T)$ as a function of resonance frequency for three different temperatures. Data are taken from Ref. 2.

Since the supercurrent in general breaks the symmetry of the underlying lattice, one expects different relaxation rates for O(2) and O(3) for a given direction of $\mathbf{p}_s$. An experiment which is able to reveal this difference in the relaxation rates is a nuclear quadrupole resonance (NQR) measurement in which the direction of a uniform supercurrent is varied.

In Fig. 5(a) we plot $1/T_1T$ for the ASF mechanism as a function of the angle ϕ between the supercurrent momentum $\mathbf{p}_s$ and the crystal axes [see Fig. 2(b)]. It follows from Eq. (9) that in the limit $T \to 0$, O(2) and O(3) $1/T_1T$ possess the same angular dependence. This identical behavior again results from the Stoner enhancement, since for the dominating particle-hole excitations with large momentum transfer $\mathbf{q}_{n,m} = \mathbf{k}_l$ (see Fig. 2), the form factors $F(q_{n,m})$ for O(2) and O(3) are the same. With increasing temperature, the relaxation rates for O(2) and O(3) begin to deviate, since excitations with smaller momentum transfer become increasingly more important, however, the maxima and minima of O(2) and O(3) $1/T_1T$ still occur at the same angle ϕ.

The relaxation rates of O(2,3) for the ESF mechanism [Fig. 5(b)], are also identical in the low-temperature limit, as follows directly from Eq. (9). However, with increasing temperature, the angular dependence of $1/T_1T$ for O(2) and O(3) is *out of phase*: the minima of O(2) $1/T_1T$ coincide with the maxima of O(3) $1/T_1T$. To demonstrate that this ''phase shift'' originates from the different form factors of O(2,3), Eq. (2), we consider the case $\phi=\pi$. One then has from Eq. (9) for O(2)

$$\frac{1}{T_1T} \sim [1+\cos^2(k_l^x/2)](D_1^2+D_4^2+2D_1D_4) + 4[1-\cos^2(k_l^x/2)]\pi^2T^2/3, \tag{12}$$

whereas for O(3) one obtains

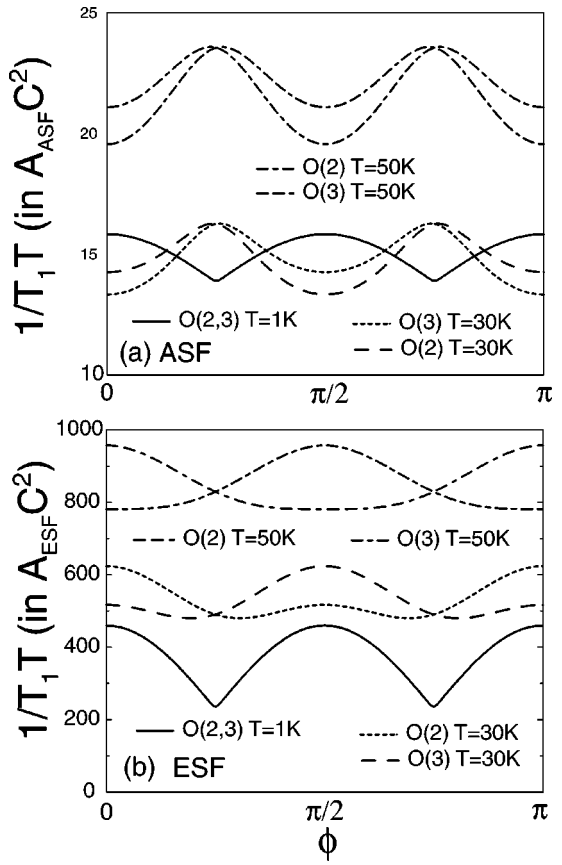

FIG. 5. ^{17}O(2,3) $1/T_1T$ for $p_s=0.02$ and three different temperatures as a function of the angle ϕ between $\mathbf{p}_s$ and the crystal x axis [see Fig. 2(b)]. (a) ASF mechanism, (b) ESF mechanism.

$$\frac{1}{T_1T}\sim[1+\cos^2(k_l^x/2)](D_1^2+D_4^2+2D_1D_4)+O(T^4). \tag{13}$$

For $T=0$ we indeed find that the O(2,3) relaxation rates are identical, while for $T>0$ (and $\phi=\pi$) O(2) $1/T_1T$ is larger than O(3) $1/T_1T$, in agreement with our numerical results in Fig. 5.

Finally, the overall scale of $1/T_1T$ within the ESF and ASF approach depends on a variety of parameters, e.g., the hyperfine coupling C, the magnetic correlations length ξ, the detailed form of the Fermi surface, etc., and is thus only insufficiently known. In contrast, we find that the frequency and temperature dependence of $1/T_1T$ are features which are qualitatively robust against changes in these parameters. Thus our predictions for the qualitative differences between the ESF and ASF relaxation mechanisms are valid for all cuprate materials, and *do not* depend on any fine-tuning of parameters.

In summary, we present a theoretical scenario for the spin-lattice relaxation rate of ^{17}O in the mixed state of the high-T_c cuprates. We consider $1/T_1$ for two relaxation mechanisms: one based on electronic spin-flip scattering of BCS-type electrons, and one due to antiferromagnetic spin fluctuations. We show that the predicted temperature and frequency dependence of $1/T_1$ differs qualitatively for these two mechanisms. A comparison of our theoretical results with the available experimental data from Ref. 2 suggests that the ASF mechanism dominates the relaxation rate. To the extent that this conclusion is confirmed by future more detailed experiments, it implies that the relaxation rate of ^{63}Cu in the mixed state is also dominated by the ASF mechanism, in contrast to the scenarios pursued in Refs. 5,7. Finally, we propose an NQR experiment in which the direction of a uniform supercurrent with respect to the crystal lattice is varied and predict a unique angular dependence of $1/T_1$ for O(2) and O(3).

It is our pleasure to thank N. Curro, W. Halperin, C. Milling, D. Pines, J. Sauls, R. Wortis, and especially C. P. Slichter for valuable discussions. This work has been supported by the Department of Energy at Los Alamos National Laboratory.

APPENDIX

The general form for $1/T_1T$ in the presence of a supercurrent is given by

$$\frac{1}{T_1T}=A\left(\frac{1}{v_Fv_\Delta}\right)^2\sum_{n,m}\{\mathcal{F}(\mathbf{q}_{n,m})G_1(D_m,D_n,T) + \mathcal{F}(\mathbf{q}_{n,m+2})G_2(D_m,D_n,T)\}, \tag{A1}$$

where $D_m=\mathbf{v}_F^{(m)}\cdot\mathbf{p}_s$, $\mathbf{v}_F^{(m)}$ is the Fermi velocity at the node in the mth quadrant of the Brillouin zone, $v_\Delta=|\partial\Delta_\mathbf{k}/\partial\mathbf{k}|$ at the nodes, and $\mathbf{q}_{n,m}$ is the momentum connecting nodes n and m. For ESF scattering we find

$$A_{\mathrm{ESF}}=\Delta S k_B(\hbar^2\gamma_n\gamma_e)^2/(2\hbar),$$

$$\mathcal{F}_{\mathrm{ESF}}(\mathbf{q}_{n,m})=F_{O(2,3)}(\mathbf{q}_{n,m}), \tag{A2}$$

while for the ASF mechanism one has

$$A_{\mathrm{ASF}}=\Delta S(\alpha g)^2k_B(\hbar^2\gamma_n\gamma_e)^2/(2\hbar),$$

$$\mathcal{F}_{\mathrm{ASF}}(\mathbf{q}_{n,m})=\frac{F_{O(2,3)}(\mathbf{q}_{n,m})}{[\xi^{-2}+(\mathbf{q}_{n,m}-\mathbf{Q})^2]^2}, \tag{A3}$$

where ΔS is a measure of the momenta in the magnetic Brillouin zone which scatter between the superconducting nodes and are relevant for the relaxation process. Since ΔS depends strongly on the exact form of the Fermi surface in the vicinity of the nodes, it is only insufficiently known. For ESF and ASF relaxation, $G_{1,2}$ is given by

$$G_1(D_m,D_n,T)=\frac{D_nD_m+\epsilon^2}{T^2}n_F(\epsilon)+\frac{\pi^2}{6} + \frac{D_n+D_m}{T}\left(\frac{\epsilon[1-n_F(\epsilon)]}{T}+\ln[n_F(\epsilon)]\right) - 2\int_0^{\epsilon/T}dx\,x\,n_F(x), \tag{A4}$$

where $n_F(\epsilon)=[\exp(\epsilon/T)+1]^{-1}$ is the Fermi function, $\epsilon=\max\{D_n,D_m\}$ and

$$G_2(D_m,D_n,T)=\frac{D_nD_m}{T^2}[n_F(D_m)-n_F(-D_n)] + \frac{D_n-D_m}{T}\left\{\frac{D_n[n_F(-D_n)-1]}{T} + \ln[n_F(-D_n)]+\frac{D_m[n_F(D_m)-1]}{T} - \ln[n_F(D_m)]\right\}+\left(\frac{D_n}{T}\right)^2 n_F(-D_n)-\left(\frac{D_m}{T}\right)^2 n_F(D_m) - 2\int_{D_m/T}^{-D_n/T} dx\, x\, n_F(x) \quad \text{for} \quad D_n+D_m\leqslant 0,$$

$$G_2(D_m,D_n,T)\equiv 0 \quad \text{for} \quad D_n+D_m>0. \tag{A5}$$

[1] N.J. Curro, Ph.D. thesis, University of Illinois at Urbana-Champaign, 1998.

[2] N.J. Curro, C. Milling, J. Haase, and C.P. Slichter, Phys. Rev. B **62**, 3473 (2000).

[3] C. Milling and C.P. Slichter (private communication).

[4] W. Halperin *et al.* (unpublished).

[5] M. Takigawa, M. Ichioka, and K. Machida, Phys. Rev. Lett. **83**, 3057 (1999).

[6] D.K. Morr and R. Wortis, Phys. Rev. B **61**, R882 (2000).

[7] R. Wortis, Ph.D. thesis, University of Illinois at Urbana-Champaign, 1997; R. Wortis, J. Berlinsky, and C. Kallin, Phys. Rev. B **61**, 12 342 (2000).

[8] We show below that the qualitative difference between ESF and ASF relaxation arises from the Stoner enhancement of the spin susceptibility which is present for the ASF mechanism, but absent for the ESF mechanism. Thus the temperature and frequency dependence of $1/T_1$ obtained in Refs. 5 and 7 agree qualitatively.

[9] M. Tinkham, *Introduction to Superconductivity* (Krieger Publishing, Boca Raton, FL, 1980).

[10] The supercurrent momentum appears in u_k, v_k, and $\Delta(k)$ only to order p_s^2.

[11] P. Monthoux and D. Pines, Phys. Rev. B **47**, 6069 (1993); D.K. Morr and D. Pines, *ibid.* **61**, R6483 (2000).

[12] D.K. Morr, J. Schmalian, and D. Pines, cond-mat/0002164 (unpublished).

[13] M.H.S. Amin, I. Affleck, and M. Franz, Phys. Rev. B **58**, 5848 (1998).

[14] For these nuclei, $\Delta(\mathbf{r})$ is uniform and $\mathbf{p}_s(\mathbf{r})$ varies sufficiently slowly which is a necessary condition for the computation of $1/T_1$ [see, e.g., P.I. Soininen *et al.*, Phys. Rev. B **50**, 13 883 (1994)]. Note, that for an applied field of $H=8$ T, only about 2% of all nuclei are located within $R=2\xi_{ab}$ from the center of the vortex core.

[15] I. Maggio-Aprile, Ch. Renner, A. Erb, E. Walker, and O. Fischer, Phys. Rev. Lett. **75**, 2754 (1995).

[16] Note that the authors of Ref. 5 assumed a square vortex lattice which is inconsistent with the experimental results of Ref. 15.

[17] Since ξ is temperature independent in the superconducting state it does not contribute to the temperature dependence of $1/T_1T$.

[18] N. Curro and C.P. Slichter (private communication).

[19] V.V. Demidov, Physica C **234**, 285 (1994).

[20] A further complication arises from the experimentally observed broadening of the ^{17}O spectrum (see the theoretical spectra in Fig. 1), whose microscopic origin still awaits further clarification (Ref. 18).